Prediction of Wetting Behaviours of Femtosecond Laser Texturized Surfaces

Ilemona Sunday Omeje*[1], Javier Prada-Rodrigo[1], Emilie Gamet[1], Yoan Di Maio[2], Raphaël Guillemet[3], Tatiana Itina[1], and Xxx Sedao[2]

[1]*Laboratoire Hubert Curien, UMR CNRS 5516, Université Jean Monnet, Université de Lyon, Saint-Etienne, France*
[2]*GIE Manutech-USD, 20 Rue Prof Benoit Lauras, Saint-Etienne, France*
[3]*Technologies & Materials Research Group, 91767 Palaiseau cedex, France*
**Corresponding author's e-mail: ilemona.sunday.omeje@univ-st-etienne.fr*

It is well known that surface topography modification can be used to tune and control the surface wettability, and femtosecond laser ablation can be applied to modify a surface's topography with ultimate precision. However, it is not so well known how to predict the surface wettability based on the surface topography produced by femtosecond laser pulses. In this communication, a simulation tool based on previously developed Level Set Method (LSM) model is developed on the commercial multiphysics software platform, COMSOL, to evaluate the wettability of polished and ultrafast laser-patterned silicon and germanium surfaces. We demonstrate its capacity for simulation of the liquid droplet evolution on various topographies of laser-textured surface. The calculations suggest that to achieve more hydrophobic behavior on laser-textured silicon and germanium, more attention should be paid to the height of the relief, and caution should be exercised when varying the period of the relief during femtosecond laser processing.

DOI: 10.2961/ilmn.2025.01.2007
Keywords: wettability, femtosecond laser, contact angle, silicon, germanium, micro-roughness, roughness factor, hydrophobic, superhydrophobic.

1. Introduction

In many modern applications, optical windows for vision applications require the light entering surface to possess multi-functionalities, such as anti-reflection, anti-fogging and self-cleaning, etc. Our recent optical simulation suggests that it is possible to create anti-reflection surface by ultrafast laser patterning of periodic sub-micrometric features [1]. On the other hand, tuning the surface topography of a sample using an ultrafast laser is known to alter its wettability rendering a surface with various desirable functionalities, such as anti-fogging and self-cleaning properties [2, 3].

The wettability of ultrafast laser-treated materials has been extensively studied. For example, Baldacchini et al. [4] and Zorba et al. [5] investigated the use of femtosecond (fs) laser irradiation to modify the wettability of silicon (Si) surfaces. By adjusting the laser fluence, they were able to control the resulting surface roughness using two different length scales (micrometre and nanometre-scale) and, consequently, the degree of hydrophobicity and superhydrophobicity. The contact angle (CA) on the laser-irradiated Si varied relatively from hydrophilic to highly hydrophobic.

Wang et al. [6] presents a method for fabricating microhole structures on germanium (Ge) surfaces using a fs laser raster-type in situ repetitive direct writing technique. The resulting microstructures exhibit excellent anti-reflective properties in the visible and near-infrared range (300-1800 nm), with an average reflectance of 2.25% compared to 41.5% for flat Ge. The microhole structures also demonstrate superhydrophobic behavior with a water contact angle of up to 133°, enabling self-cleaning capabilities. It is well established that to achieving a suitable wettability depends on both the surface topography and the chemical composition [7].

In recent decades, the effect of surface roughness on wettability has been explained by two main theories: the Wenzel and Cassie-Baxter model [8, 9]. Meanwhile, the role of chemical composition on wettability is still under investigation and it is a hot research topic most especially in the laser community [10-13]. The Wenzel model applies when the liquid fully penetrates the surface roughness, leading to enhanced wettability for hydrophilic surfaces and decreased wettability for hydrophobic surfaces [8]. On the other hand, the Cassie-Baxter model describes a scenario where the liquid rests on a composite surface of solid and air pockets, typically resulting in increased hydrophobicity [9].

The Cassie-Baxter model accurately describes surfaces that are superhydrophobic. However, these superhydrophobic surfaces can become unstable due to factors like vibration, evaporation, air diffusion, and droplet impact [14-17]. These factors can lead to a transition from the Cassie-Baxter state to the fully wetted Wenzel state, resulting in the loss of superhydrophobicity [14, 16, 18]. Often, there can be a co-existent between these two states, and this is generally known as the metastable state [18-20]. Moreover, the transition from the Cassie-Baxter to the Wenzel state may not always be instantaneous and can occur gradually over a variable time scale [21]. Depending on the nature of the rough surface, this transition can lead to dynamic wetting, where the contact angle changes as the droplet moves [22]. This behavior, known as contact angle hysteresis, occurs when the contact angle differs between the advancing and receding edges of the droplet [23].

In addition, the Wenzel and Cassie-Baxter models have limitations in accurately predicting the contact angle and behavior of liquids on surfaces with extreme roughness. These models often fail to account for the detailed variations in surface structure and the dynamic interactions at the micro and nanoscale [24, 25]. Hence, numerical modeling serves as a viable approach to accurately predict the contact angle and wetting dynamics on various surfaces. Numerical simulations can incorporate detailed surface topography and interactions, providing a more comprehensive understanding of wetting phenomena on rough surfaces.

Various numerical approaches were used in wettability studies. For instance, Han et al. [26] investigated the wettability and numerical modeling of Si surfaces with different microstructures using a volume−of−fluid approach. Their study highlights the limitations of traditional models like Wenzel and Cassie−Baxter in predicting wettability on complex microstructured surfaces. Additionally, the authors emphasize the effectiveness of this numerical approach in providing accurate predictions of contact angles by incorporating detailed surface topography and interactions at the micro and nanoscale.

In our recent study [27], we numerically investigated the impact of laser-textured surfaces on the wetting dynamics of water droplet using the LSM. Our findings show that surface patterns significantly influence droplet spreading and CA, with complex patterns leading to decreased wettability. We also studied the effects of impact velocity and viscosity on droplet behavior, revealing that higher velocities increase spreading, while higher viscosities decrease it. These findings have important implications for the design of surfaces with controlled wettability for different applications. In this follow-up study, we aim to extend the modeling tool to numerically evaluate the wettability of laser-patterned surfaces. The objective is to predict the wetting performance of various surface topography designs from optical simulations, with the ultimate goal of designing a multifunctional surface.

Table 1 The laser conditions used for the creation of the topographies on Si and Ge.

Sample	Number of pulses	Fluence (J/cm^2)	Pitch (µm)
Si	20	58	25
Ge	10	58	25

2. Materials and methods

The experimental part of the study was performed onto 2 different semiconductors that are commonly used in microelectronics industry, namely mono-crystalline Si and Ge. The characteristics of the materials are as follows: Si wafers (1 0 0) of 1 mm thick that were polished on both sides, pure Ge wafers (1 0 0) of 1 mm in thickness that were polished in both sides also. The initial surface roughness Ra of both materials is well below 1 nm. The creation of the surface topographies was realized by using ultrafast laser ablation. We positioned the samples with respect to the laser processing platform using motorized XYZ translation stages from NewPort, Micro-Controle Spectra-Physics S.A.. A commercially available ultra-violet (UV) laser system (of Monaco model from Coherent Inc.) was used to created surface structures. The Monaco UV laser system, operating at 343 nm wavelength, provides 350 fs pulses at a repetition rate of 10 kHz. All pulses were focused through a f/θ with the nominal focal length of 100 mm and a spot diameter of 8.5 µm (the diameter was determined experimentally). The laser fluence was adjusted using a half-wave plate (λ/2) associated with a polarizer. The pulse energy was measured with a thermopile power-meter (Gentec Inc.). The laser conditions used for the creation of the topographies for this study are summarized in Table 1.

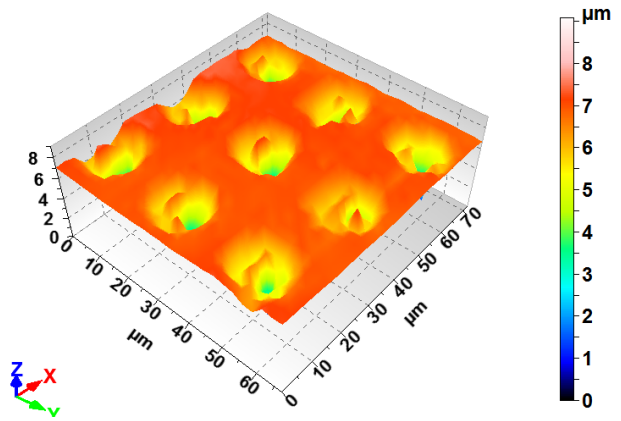

Fig. 1 A typical surface topography created using femtosecond laser pulses.

For surface geometry evaluation, a confocal microscope (Stil, from Altimet) was used for surface topography measurements [28]. A typical surface topography produced on Si after UV fs laser irradiation is presented in Fig. 1. Individual craters were created on the Si surface and the topographical characteristics such as crater diameter, depth, pitch distance etc, are related to the laser spot size, laser fluence, number of laser pulses, and predefined crater-to-crater spacings. For detailed geometrical values of the craters on the Si and Ge samples, 2D surface profiles are extracted from the confocal measurement. A typical 2D profile of the surface relief across the surface patterns is shown in Fig.2(b). The wettability measurements were carried out with a laboratory-developed system within the Manutech-USD consortium [29]. They were performed in a controlled atmosphere (temperature (T) being 22.95 ± 0.45°C, and relative humidity (RH) being 40 ± 8 %). A 3 µL droplet of demineralized water was deposited on the surface, and the evolution of the droplet shape was visualized with a camera and a sample rotation stage enabling 360° inspection and CA measurements. The platform moved at a speed of 0.1 rad/s. The droplet profile and especially the CA were extracted from the complete droplet 360° of rotation leading to approximately 80 measurements per droplet. The first CA measurements were carried out immediately after laser processing and it was shown that all the samples exhibiting hydrophilic properties [30]. The second step of CA measurements was performed on the same samples, a few months after the laser patterning process, and more specifically after a thermal treatment procedure in which the samples received an ultrasonic bath cleaning (demineralized water for 15 min), and an autoclave treat-

ment at 90°C for 45 min. The data represent the measurements from 4 consecutive, individuals and contact-less droplets on each surface.

3. Modeling details

Our present study is based on a model designed to simulate the behavior of two-phase flow on flat Si, and Ge surfaces, focusing on the interaction between immiscible fluids, such as air and a water droplet as shown in Fig. 2 (a). An important aspect of our model is the inclusion of surface tension effects, which play a significant role in governing the behavior of fluid interfaces. Surface tension forces are calculated using a specialized expression involving gradient terms, a surface tension coefficient, and the Dirac delta function, allowing us to accurately capture the dynamics at the fluid-solid interface.

$$r = 1 + \frac{2h}{p}; p = w + s. \qquad (1)$$

To track the interface between the two immiscible fluids, we employed the conservative LSM. This method utilizes a level-set function, which smoothly transitions between 0 (indicating air) and 1 (indicating water droplet), effectively depicting the fluid interface. Implementation of the model was carried out using a finite-element solver discretized in COMSOL Multiphysics 6.0 software, facilitating precise numerical computation. Our simulations were conducted in 2D axis-symmetry to reduce computational cost while maintaining accuracy.

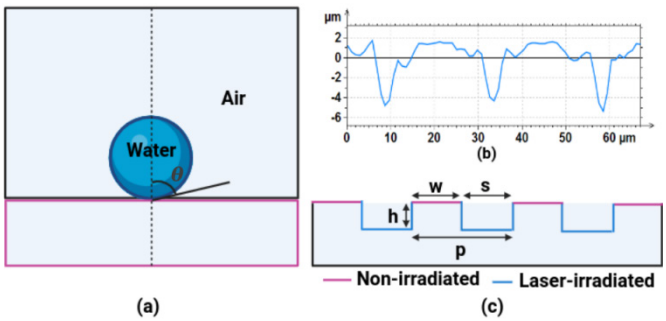

Fig. 2 (a) Asymmetry simulation setup of water droplet with a diameter of 1 mm on a flat surface. (b) 2D topography profile created by femtosecond laser. (c) A 2D parametric geometrical patterned displaying both non-irradiated spots and laser-irradiated spots with varying heights (h), widths (w), groove widths (s), and a period (p) of the relief.

Boundary conditions were carefully chosen to ensure realistic simulation outcomes. Open boundary conditions with zero pressure were applied to all boundaries except the wetted wall, where equilibrium CA was employed to define the surface wettability. To prevent singularity problem at the wetted wall, we adopted the Navier slip boundary condition, supplemented by a frictional force term on the liquid-solid interface. This approach ensured numerical stability and accuracy throughout the simulation process. More details about the modeling set-up, implementation and validation of water droplet on flat surface can be found in [27].

Subsequently a laser-textured pattern, featuring heights (h), widths (w), groove widths (s), and a periodicity (p) as depicted in Fig. 2 (c), was introduced on the two surfaces [31, 32]. The structural parameters h, w, s, and p are adjustable based on the topography profile of the laser-patterned surfaces. For the sake of simplicity, we have only explored the cases where w=s. The adjustable parameters used in the prediction of the wettability are shown in Table 2. To facilitate the adjustment of these parameters, we use the roughness factor (r) to quantify them, as shown in Eq. 1. The CA was then plotted against r. In order to interpret the relationship between r and CA, a simple linear regression analysis was performed [33]. The coefficient of determination, R^2, was used as the goodness of fit to measure how well the linear regression model explains the variability of the data [34].

The diameter of the water droplet corresponds to that used in the experimental setup, which is 1 mm. It is important to mention that the density, dynamic viscosity, and surface tension values for both water and air are sourced from Sikalo et al. [35, 36]. Water has a density of 996 kg/m^3, a dynamic viscosity of 0.001 Pa.s, and the surface tension between air and water is 0.073 N/m. In comparison, air has a density of 1.204 kg/m^3 and a dynamic viscosity of 1.814 x 10^{-5} Pa.s. The simulation of water droplets on the two flat surfaces, as well as on the laser-patterned surface, was carried out for 100 microseconds. This duration is sufficient for the water droplets to reach an equilibrium state.

Table 2 Values of the adjustable parameters of laser-textured patterned introduced on Si and Ge.

Si	p (mm)	h (mm)	r	Ge	p (mm)	h (mm)	r
1	25	0	1	1	25	0	1
2	25	2	1.16	2	25	2	1.16
3	25	5	1.40	3	25	5	1.40
4	25	7.3	1.58	4	25	6.5	1.52
5	25	10	1.80	5	25	10	1.80
6	25	13	2.04	6	25	13	2.04
7	25	16	2.28	7	25	16	2.28
8	10	0	1	8	10	0	1
9	10	7.3	1.58	9	10	6.5	1.52
10	15	7.3	1.63	10	15	6.5	1.57
11	18	7.3	1.73	11	18	6.5	1.65
12	20	7.3	1.81	12	20	6.5	1.72
13	23	7.3	1.97	13	23	6.5	1.87
14	25	7.3	2.46	14	25	6.5	2.30

4. Results and discussion

In this section we present our results as follows: firstly we discuss the initial state of Si and Ge, in terms of surface roughness and surface wettability; and then we move on to the wettability evolution once the surface topography is produced onto the Si and Ge surface by fs laser pulses; after that, we expand our discussion to the influential factors that governing the wettability performance; in the end we make comment on the shortcoming of current approach as well as project our perspective for future development.

4.1 Equilibrium contact angle on Si and Ge

Fig. 3 presents snapshots of a 1 mm water droplet on flat Si and Ge substrates, compared with the results from both simulation and experimental methods. For the flat Si substrate, the simulated equilibrium CA of 29.4° is very close to

the experimental CA of 28.85°, with a small difference of 0.55°. Similarly, for the Ge substrate, the simulated equilibrium CA of 63.72° closely matches the experimental CA of 63.60°, with an even smaller difference of 0.12°. The close agreement between the simulation and experimental results validates the accuracy and reliability of the numerical model used in these simulations and as reported in [27]. This validation implies that the model can be trusted to predict the behavior of water droplets on similar surfaces with a high degree of precision.

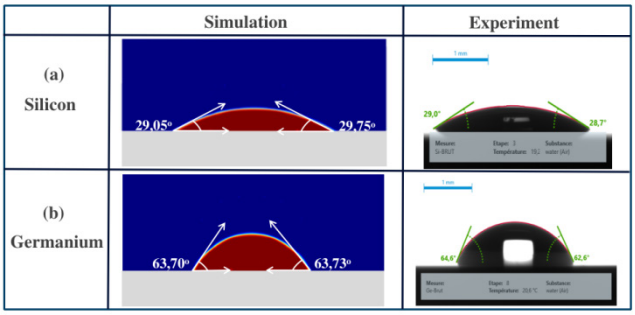

Fig. 3 Comparison of (a) simulation and (b) experimental results of water droplets with a diameter of 1 mm on flat Si, and Ge substrates.

4.2 Equilibrium contact angle on laser patterned Si and Ge

Fig. 4 represents the scale plots of simplified, idealized surface profiles based on the experimental µm topography measurements for laser-patterned substrates which are used as input in the simulation to study the effect of the microstructure on the droplet... For Si, the measurements were: p = 25 µm, w = 12.5 µm, and h = 7.3 µm as shown in Fig. 4 (a). For Ge, the measurements were: p = 25 µm, w = 12.5 µm, and h = 6.5 µm as shown in Fig. 4 (b). The corresponding r value for Si relief features is 1.58 and that of Ge is 1.52 respectively.

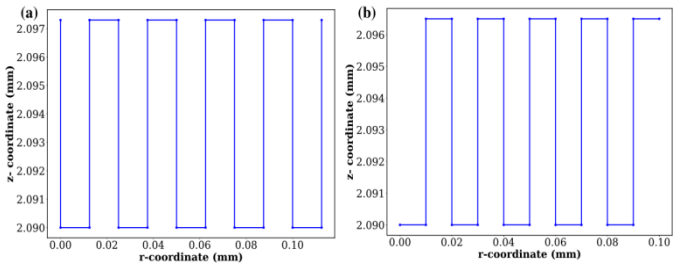

Fig. 4 Simplified surface profile based on experimental topography measurements for laser-patterned substrates. (a) For Si, the measurements were: p = 25 µm, w = 12.5 µm, and h = 7.3 µm. (b) For Ge, the measurements were: p = 25 µm, w = 12.5 µm, and h = 6.5 µm.

Fig. 5 (a) shows a snapshot of the equilibrium CA of a water droplet on micro-relief Si of both simulation and experiment. The simulation results show an equilibrium CA of 109.55°, while the experimental measurements indicate a slightly lower CA of 104.8°. This close agreement suggests that the simulation model is quite accurate, with only a minor difference of 4.75°. Similarly, Fig. 4 (b) presents the equilibrium CA of a water droplet on Ge. Here, the simulation predicts an equilibrium CA of 115.62°, whereas the experimental value is 104.3°. The difference between these values is 11.32°, which is slightly larger than the discrepancy observed for Si. The observed differences between the simulated and experimental CAs for both Si and Ge can be attributed to the presence of native oxides on the surfaces between the relief features created by fs laser texturing. These native oxides can alter the surface chemistry thus, affecting the wettability of the surfaces [6, 37, 38].

In addition, the simulations reveal that there is an air gap between the water droplet and the relief features for laser-textured Si and Ge. The water droplet does not fully penetrate the micro-relief structure, leading to incomplete wetting of the surface. The introduction of micro-roughness through laser patterning transforms the surfaces of both Si and Ge from a hydrophilic state, when the surfaces are flat, to a hydrophobic state, when the surfaces are textured with relief features. This change in wettability is important for optical windows applications where controlling the wetting properties is essential.

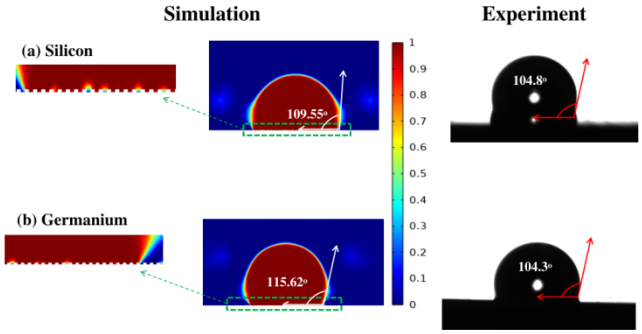

Fig. 5 Snapshot of (a) simulation and (b) experiment showing a water droplet on laser-patterned Si with micro-relief measurements of p = 25 µm, w = 12.5 µm, and h = 7.3 µm, and on Ge with measurements of p = 25 µm, w = 12.5 µm, and h = 6.5 µm. The color bar in the simulation represents the fluid interface, where a value of 0 corresponds to air and a value of 1 corresponds to the water droplet, as defined by the LSM.

The wetting behavior observed on laser-textured Si and Ge can be described as a Wenzel-Cassie-Baxter state. In this state, the water droplet partially penetrates the micro-relief features but does not completely fill them, resulting in the trapping of air bubbles between the droplet and the surface. The formation of air bubbles at the solid-liquid interface occurs due to the air pressure present in the gaps between the micro-relief features [39, 40]. Figure 6 illustrates the air pressure distribution between the water droplet and the micro-reliefs of both Si and Ge surfaces.

Additionally, for the laser-patterned Si, the air pressure beneath the water droplet is measured at 6260 Pa. In comparison, the air pressure for the laser-patterned Ge is slightly lower, at 4600 Pa. These high air pressures are a result of the trapped air in the micro-reliefs, which significantly influences the droplet's behavior on the textured surfaces.

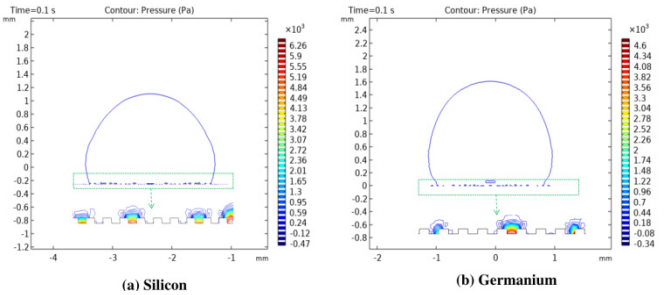

(a) Silicon (b) Germanium

Fig. 6 Air pressure in the gaps between the micro-reliefs of Si with surface features of p = 25 µm, w = 12.5 µm, h = 7.3 µm and Ge with surface features of p = 25 µm, w = 12.5 µm, and h = 6.5 µm.

Because of the air pressure beneath the relief features, the water droplet is effectively trapped on the micro-reliefs of both Si and Ge surfaces. This trapping mechanism causes the droplet to reach an equilibrium state more rapidly compared to when it is on a flat surface. The presence of air bubbles prevents the water droplet from completely filling the micro-relief gaps, leading to a change in the contact angle. The increased contact angle observed on the textured surfaces of Si and Ge is a direct consequence of this trapped air. The high air pressure supports the droplet, maintaining a larger angle of contact with the surface. This phenomenon is indicative of the transition from a hydrophilic state, observed on flat surfaces, to a hydrophobic state, because of the micro-roughness created by laser patterning.

4.3 Wettability behavior of laser-treated Si and Ge surfaces with varying topography

Fig. 7 shows the Plot of CA as a function of the r for (a) Si with constant micro-relief p of 25 µm, with varied h of 2 - 16 µm and (b) constant h of 7.3 µm with varied p of 10 - 25 µm. (c) Ge with surface features of constant p of 25 µm, with varied h of 2 - 16 µm, and (d) constant h of 6.5 µm with varied p of 10 - 25 µm. A full detail of these adjusted parameters is shown in Table 2.

In Fig. 7 (a), the CA increases with the r, indicating that increased roughness transforms the Si surface from hydrophilic to hydrophobic state. This trend is evident as the CA shows a significant rise from r = 1.8 to r = 2.46. The strong correlation between r and CA is highlighted by the R^2 of 0.87, suggesting that varying the h while keeping the micro-relief p constant favors wettability changes. In Fig. 7 (b), the CA also shows an increasing trend with r, but the relationship is less straightforward compared to Fig. 7 (a). There are more fluctuations in the CA values, with the highest CA occurring at r = 2.46. Despite the surface transition from hydrophilic to hydrophobic, the moderate correlation, indicated by an R^2 value of 0.71, suggests that the trend of wettability is less predictable when h is fixed and p is varied.

Fig. 7 (c) reveals the results for the case when the CA increases with r, similar to the trend observed in Fig. 7 (a). As r rises, the Ge surface transitions from hydrophilic to a superhydrophobic state. This significant shift is particularly noticeable between r = 1.8 and r = 2.28. The strong correlation between r and CA is shown by an R^2 value of 0.89, indicates that modifying the h while maintaining a constant micro-relief p effectively influences wettability. This supports the observations made for Si surfaces in Fig. 7 (a). In contrast, Fig. 7 (d) reveals a more complex relationship between CA and r, similar to the results shown in Fig. 7 (b). While there is an overall increase in CA with higher r, the relationship is less straightforward and shows more variability. The highest CA values are found between r = 1.87 and r = 2.3. In addition, the strong correlation, reflected in an R^2 value of 0.86, indicates that predicting wettability trends is more challenging when h is fixed and p is varied. The findings for Si surfaces also confirm this statement, as shown in Fig. 7 (b).

Moreover, in Fig. 7(c) and 7(d), the simulations predict CAs nearing 180°, indicating extreme superhydrophobic behavior under specific parameter configurations. These results are theoretical predictions based on idealized surface conditions, including uniformity and periodicity of microstructures. While achieving such high contact angles experimentally is challenging, these simulations highlight the potential upper limits of surface hydrophobicity. It is essential to emphasize that real-world surfaces, influenced by imperfections and dynamic effects, may not achieve these extreme angles. Future experimental validation and model refinements are necessary to confirm these predictions and further explore the practical implications of such surface designs.

Thus, using only r as the main parameter, as it was often done, is an oversimplification in the case of a textured relief. Instead, structure depth and period should be used as independent parameters since different R^2 were obtained for Fig. 7 (a) and (b) and for Fig. 7 (c) and (d). This result can be attributed to the differences in the roles of these parameters in the determination of the actual contact area, interaction energy and other important surface characteristics.

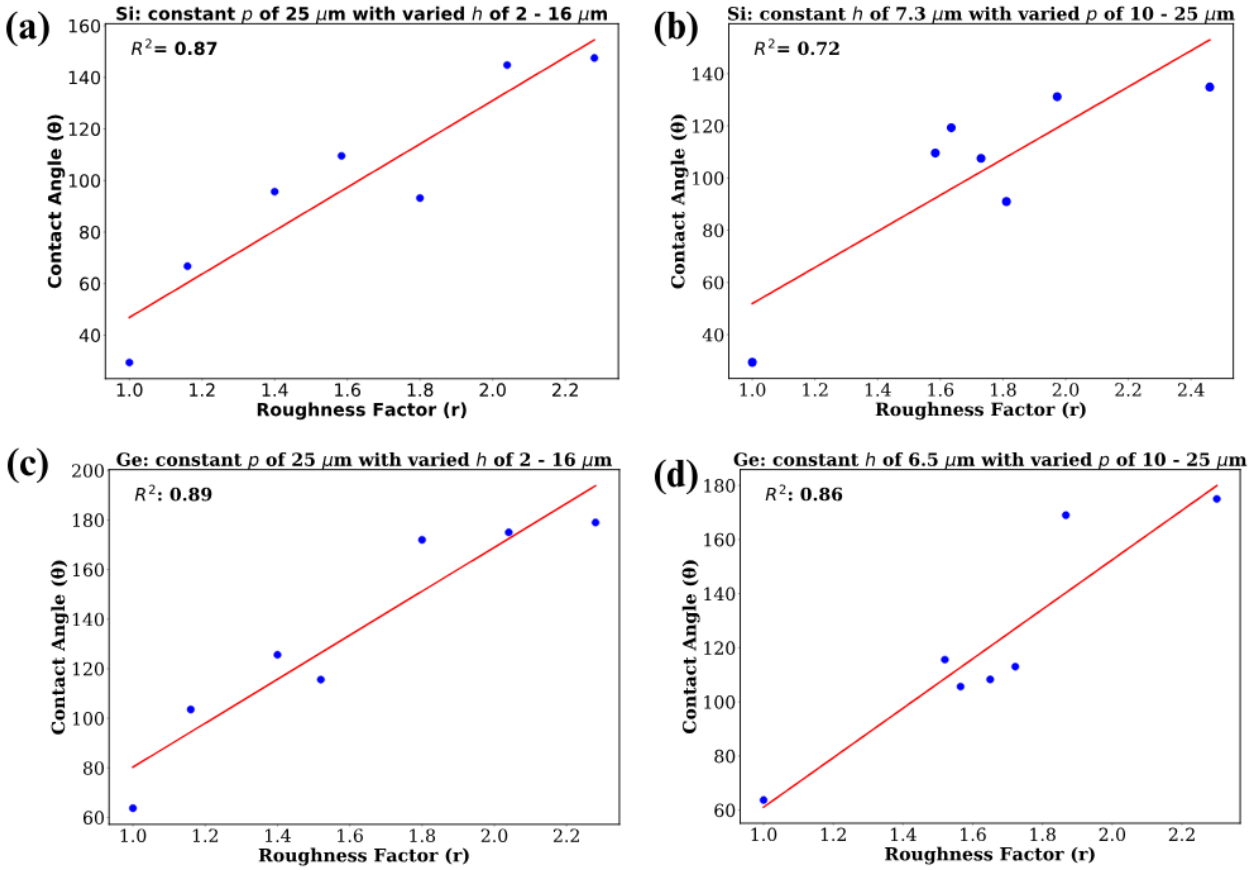

Fig. 7 Plot of contact angle as a function of the roughness factor for (a) Si with constant micro-relief p of 25 μm, with varied h of 2 - 16 μm and (b) constant h of 7.3 μm with varied p of 10 - 25 μm. (c) Ge with surface features of constant p of 25 μm, with varied h of 2 - 16 μm, and (d) constant h of 6.5 μm with varied p of 10 - 25 μm.

In general, to achieve more hydrophobic behavior on laser-textured Si and Ge, more attention should be paid to the h of the relief, and caution should be exercised when varying the p during fs laser processing. It is important to note that a current limitation of this simulation is the exclusion of dynamic wetting phenomena. To reach a more comprehensive understanding of wettability on micro-textured surfaces, future modeling approaches and experiments should incorporate the study of both advancing and receding contact angles. This will allow for a more accurate assessment of the droplet's dynamics and stability on the surface.

It is important to mention that the current simulation does not account for the role of surface chemistry, which is a critical factor in determining wettability. Surface chemistry can significantly influence the interaction between the liquid and the solid surface, affecting the CA and overall wettability. However, integrating chemical effects into the finite element approach used in COMSOL Multiphysics presents considerable challenges, as this method primarily focuses on physical and geometric aspects.

To address the influence of surface chemistry, alternative computational techniques such as Density Functional Theory (DFT) [41] and molecular dynamics (MD) simulations [31, 32] should be considered. DFT can provide insights into the electronic structure and chemical properties of the surface, while MD simulations can model the interactions between molecules at the atomic level. These approaches can capture the interaction between surface chemistry and wettability, offering a more holistic understanding of the factors that govern droplet behavior on micro-textured surfaces. In addition to the future prospects of this work, instead of using a parametric profile for the wetting simulation, a customized or in-house code can be developed to directly incorporate the 2D topography profile from fs laser texturing as a structured profile in the COMSOL simulation. Taking the highlighted points into consideration will lead to a more robust and realistic model. This, in turn, will improve the accuracy of predictions related to droplet dynamics and wettability on micro-textured surfaces, ultimately informing better design and optimization of materials for various applications.

5. Conclusion

This study presents a numerical model to predict the optimal laser-textured geometries for surface wettability modification, primarily focusing on sub-micrometric features on Si and Ge, using the LSM developed in previous work. The model simulates the interaction between immiscible fluids, such as air and water droplets, allowing for an accurate capture of the dynamics at the fluid-solid interface. The model has been validated by comparing the simulations with experimental results, demonstrating a high degree of precision in predicting water droplet behavior on similar surfaces.

Micro-relief measurements from laser-textured experiments were used as inputs in the simulation in the form of parametric surfaces, and wettability tests were performed. The simulation results showed good agreement with experimental data, with minimal deviation. Specifically, the introduction of micro-roughness through laser patterning transformed the surfaces from a hydrophilic state, when flat, to a hydrophobic state with relief features.

The study also demonstrates simulation of various topographies, including fixed height of the relief with varying periods of the laser-textured surface, and vice versa. The calculations revealed that to achieve more hydrophobic behavior on laser-textured Si and Ge, more attention should be paid to the height of the relief, and caution should be exercised when varying the period of the relief during femtosecond laser processing.

Acknowledgments

This work was supported by the French National Research Agency (ANR) under the project Last-Flow (ANR-22-CE24-0026-01). We gratefully acknowledge the financial support and resources provided by the ANR, which have been crucial in advancing our research. We wish to also acknowledge the support of National French Ministry of Education. We are thankful to the support provided in part by EUR Manutech Sleight and Labex Manutech-SISE. We are grateful to Pauline Pavia and Antoine Gonon from GIE Manutech-USD for their assistance in wetting measurements.

List of common abbreviations

fs - femtosecond
LSM - Level Set Method
Si – Silicon
Ge - Germanium
CA - Contact angle
r – Roughness factor
p – Period of the relief
h – Height of the relief
μm – Micrometer
R^2 – Coefficient of determination

References

[1] T. Kämpfe, L. Dubost, and X. Sedao: Dispositif optique wo2021079077, Patent 0, (2021) 0.
[2] K. Maghsoudi, E. Vazirinasab, G. Momen, and R. Jafari: Ind. Eng. Chem. Res., 59, (2020) 9343.
[3] I. Firkowska-Boden, X. Zhang, and K. D. Jandt: Adv. Healthc. Mater., 7, (2018) 1700995.
[4] T. Baldacchini, J. E. Carey, M. Zhou, and E. Mazur: Langmuir, 22, (2006) 4917.
[5] V. Zorba, L. Persano, D. Pisignano, A. Athanassiou, E. Stratakis, R. Cingolani, P. Tzanetakis, and C. Fotakis: Nanotechnology, 17, (2006) 3234.
[6] K. Wang, Y. Zhang, J. Chen, Q. Li, F. Tang, X. Ye, and W. Zheng: Coatings, 14, (2024) 262.
[7] J. Yong, F. Chen, Q. Yang, and X. Hou: Soft Matter, 11, (2015) 8897.
[8] R. N. Wenzel: Ind. Eng. Chem. Res., 28, (1936) 988.
[9] A. Cassie and S. Baxter: Trans. Faraday Soc., 40, (1944) 546.
[10] G. Giannuzzi, C. Gaudiuso, R. Di Mundo, L. Mirenghi, F. Fraggelakis, R. Kling, P. M. Lugarà, and A. Ancona: Appl. Surf. Sci., 494, (2019) 1055.
[11] M. Moze, M. Zupancic, M. Hocevar, I. Golobic, and P. Gregorcic: Appl. Surf. Sci., 490, (2019) 220.
[12] P. Bizi-Bandoki, S. Valette, E. Audouard, and S. Benayoun: Appl. Surf. Sci., 273, (2013) 399.
[13] A. O. Ijaola, E. A. Bamidele, C. J. Akisin, I. T. Bello, A. T. Oyatobo, A. Abdulkareem, P. K. Farayibi, and E. Asmatulu: Surf. & Interfac., 21, (2020) 100802.
[14] D. Bartolo, F. Bouamrirene, E. Verneuil, A. Buguin, P. Silberzan, and S. Moulinet: EPL, 74, (2006) 299.
[15] Z. Yoshimitsu, A. Nakajima, T. Watanabe, and K. Hashimoto: Langmuir, 18, (2002) 5818.
[16] Y. C. Jung and B. Bhushan: Langmuir, 25, (2009) 9208.
[17] G. McHale, S. Aqil, N. Shirtcliffe, M. Newton, and H. Y. Erbil: Langmuir, 21, (2005) 11053.
[18] D. Bonn: COCIS, 6, (2001) 22.
[19] W. Ren, Langmuir: 30, (2014) 2879.
[20] A. Giacomello, M. Chinappi, S. Meloni, and C. M. Casciola: Phys. Rev. Lett., 109, (2012) 226102.
[21] P. Lv, Y. Xue, Y. Shi, H. Lin, and H. Duan: Phys. Rev. Lett., 112, (2014) 196101.
[22] M. Ramiasa, J. Ralston, R. Fetzer, and R. Sedev: Adv. Colloid Interface Sci., 206, (2014) 275.
[23] H. Kusumaatmaja and J. Yeomans: Langmuir, 23, (2007) 6019.
[24] G. McHale: Langmuir, 23, (2007) 8200.
[25] H. Y. Erbil and C. E. Cansoy: Langmuir, 25, (2009) 14135.
[26] S. Han, R. Yang, C. Li, and L. Yang: Appl. Sci.,9, (2019) 566.
[27] I. S. Omeje and T. E. Itina: Appl. Surf. Sci. Adv., 9, (2022) 100250.
[28] D. Pallarés-Aldeiturriaga, P. Claudel, J. Granier, J. Travers, L. Guillermin, M.-O. Flaissier, P. B. d'Augeres, and X. Sedao: Micromachines, 12, (2021).
[29] D. Pallarés-Aldeiturriaga, S. Papa, A. A. Khalil, A. Pascale-Hamri, M. Maaluf, Y. D. Maio, A. Guignandon, V. Dumas, and X. Sedao: Appl. Phys. A, 128, (2022) 100.
[30] A. Ouchene, G. Mollon, M. Ollivier, X. Sedao, A. Pascale-Hamri, G. Dumazer, and E. Serris: Appl. Surf. Sci., 630, (2023) 157490.
[31] D. Niu and G. Tang: Int. J. Heat Mass Transf., 79, (2014) 647.
[32] J. Zhao, B. Wang, Y. Pan, W. Wang, and C. Zhao: Chem. Phys. Lett., 785, (2021) 139161.
[33] D. Maulud and A. M. Abdulazeez: JASTT, 1, (2020) 140.
[34] J. P. Barrett: Am. Stat, 28, (1974) 19.

[35] S. Sikalo, H.-D. Wilhelm, I. Roisman, S. Jakirlić, and C. Tropea: Phys. Fluids, 17, (2005).
[36] Š. Sikalo and E. Ganić: Exp. Therm. Fluid. Sci., 31, (2006) 97.
[37] B. Nunes, A. Serro, V. Oliveira, M. Montemor, E. Alves, B. Saramago and R. Colaço: Appl. Surf. Sci., 257, (2011) 2604.
[38] S. Stroj, S. Kasemann, M. Domke, G. Piredda, J. Zehetner, and V. Matylitskaya: Appl. Surf. Sci., 420, (2017) 550.
[39] V. Mehdi-Nejad, J. Mostaghimi, and S. Chandra: Phys. Fluids,15, (2003) 173.
[40] S. Thoroddsen, T. Etoh, K. Takehara, N. Ootsuka, and Y. Hatsuki: J. Fluid Mech., 545, (2005) 203.
[41] A. Hodgson and S. Haq: Surf. Sci. Rep., 64, (2009) 381.

(Received: June 28, 2024, Accepted: February 24, 2025)